

Received 12 October 2024, accepted 3 November 2024, date of publication 12 November 2024, date of current version 3 December 2024.

Digital Object Identifier 10.1109/ACCESS.2024.3496656



Load Demand Modeling of Large-Scale Charging Infrastructure for Electric Vehicles In-Motion

TRAVIS NEWBOLT[©]¹, (Graduate Student Member, IEEE), MCKAY WAITE², (Graduate Student Member, IEEE), PARAS MANDAL[©]¹, (Senior Member, IEEE), HONGJIE WANG[©]², (Senior Member, IEEE), AND REGAN ZANE[©]², (Senior Member, IEEE)

¹Department of Electrical and Computer Engineering, The University of Texas at El Paso, El Paso, TX 79968, USA ²Department of Electrical and Computer Engineering, Utah State University, Logan, UT 84322, USA

Corresponding author: Paras Mandal (pmandal@utep.edu)

This work was supported in part by the National Science Foundation (NSF) through the Advancing Sustainability through Powered Infrastructure for Roadway Electrification (ASPIRE) Engineering Research Center under Award 1941524 and Faculty Early Career Development Program (CAREER) Award 2239169, and in part by the Department of Energy/the National Nuclear Security Administration under Award DE-NA0004016.

ABSTRACT As electric vehicles (EVs) become increasingly common in transportation infrastructures, the need to strengthen and diversify the EV charging systems becomes more necessary. Dynamic Wireless Power Transfer (DWPT) roadways allow EVs to be recharged while in-motion, thus allowing to improve the driving ranges and facilitating the widespread adoption of EVs. One major challenge to adopt large-scale DWPT networks is to efficiently and accurately develop load demand models to comprehend the complex behavior on power distribution grid due to difficulty in developing power electronic simulations for charging systems consisting of either numerous transmitter pads or high traffic volumes. This paper proposes a novel modified Toeplitz convolution method for efficient large-scale DWPT load demand modeling. The proposed method achieves more accurate modeling of DWPT systems from a few transmitter pads to tens of miles in real-world traffic scenarios with light computational load. Test results for a small-scale DWPT system are first generated to validate the accuracy of the proposed method before scaling to large-scale load demand modeling where real-world traffic flow data is utilized in DWPT networks ranging from 2—10 miles. A comparative analysis is further performed for the scenarios under consideration to demonstrate the efficiency and accuracy of the proposed method.

INDEX TERMS Convolution method, dynamic wireless power transfer, electrified transportation, EVs charging load, power distribution system.

NOMENCLATURE

- α Length of transmitter pads.
- β Rated power capacity of receiver pad.
- β' Rated power capacity of transmitter pad.
- δ Length of receiver pad.
- ϵ Receiver and transmitter pad overlap percentage.
- λ Horizontal distance between transmitter pads.
- ϕ Phase Shift of Gate Signals.
- ρ Power output fitting variable.

The associate editor coordinating the review of this manuscript and approving it for publication was Alon Kuperman¹⁰.

- C_{pp} Primary Parallel Capacitance.
- C_{ps} Primary Series Capacitance.
 - C_{sp} Secondary Parallel Capacitance.
- C_{ss} Secondary Series Capacitance.
- L_p Primary Inductance.
- L_s Secondary Inductance.
- L_{ps} Primary Series Inductance.
- L_{ss} Secondary Series Inductance.
- M Mutual Inductance.
- *m* Total distance to traverse.
- N Current position of vehicle.
- *n* Total length of charging system.



 P_A Cross-sectional area output array. P_R Power transference output array.

 S_R Receiver matrix. S_T Transmitter matrix. T_R Modified Toeplitz matrix. V_{bat} EV Battery Voltage.

 $V_{\rm in}$ Transmitter Input Voltage (dc).

CONV Convolution.

DWPT Dynamic Wireless Power Transfer.

ES Euclidean Similarity.

ETN Electrified Transportation Network.

EV Electric Vehicle. HDV Heavy-duty Vehicle.

INTG Integrative.

LDV Light-Duty Vehicle.
MAE Mean Absolute Error.

mCONV Modified Toeplitz Convolution.

MDV Medium-duty Vehicle.
PT Power Transmitter.
Rx Receiver Pad.
TF Traffic Flow.
Tx Transmitter Pad.

I. INTRODUCTION

Recent advancements in Electrified Transportation Networks (ETNs) are addressing the growing need to provide clean, sustainable, and reliable energy to charge Electric Vehicles (EVs) for reducing petroleum fuel consumption. The ETN development requires the collaboration of multiple disciplines, such as power electronics, power systems, and transportation engineers to design adequate infrastructure to facilitate the complete transition to EVs. Currently, it is estimated that EV sales will reach 2.9 million by 2030 and has experienced a sales increase of approximately 50% between the years 2022 and 2023 [1], [2]. With this, it's reasonable to expect electrical load demands to fluctuate proportionally with EV sales as their density into transportation networks increase. This will potentially require a modernization of electrical equipment, i.e., distribution lines, transformers, feeders and etc., to prevent any hazardous events from occurring that could cause grid failure. The most common charging access point for EVs are located at residential locations that implement plug-in power transfer architectures. However, these systems produce slow charging speeds and causes electrical load demands present on distribution grids to increase before and after normal business hours [3], [4], [5], [6], [7]. Commercial fast-chargers offer higher charging speeds ranging between 15 minutes to 1-hour through higher power capacities, but due to the minimal availability of chargers queuing will inevitably lengthen the amount of time required to charge [8], [9], [10]. These charging speeds are not comparable with internal combustion engine vehicles and has developed a phenomenon in human behavior known as range anxiety that will decrease the adoption of EVs [11], [12]. Dynamic Wireless Power Transfer (DWPT) networks, which allows EVs to be charged while in-motion, are gaining great attention as it can achieve increased EV ranges without increasing the battery size while also reducing the consumption of petroleum fuels enabling air quality and noise pollution to be mitigated [13], [14], [15], [16].

Generally, capacitive and inductive power transfers are the types of DWPT infrastructures utilized [17], [18], [19], [20]. In practice, however, the majority of DWPT infrastructures are inductive wireless power transfer implemented through consecutively embedded inductive coils, which are referred to as transmitter (Tx) pads, within a roadway, and a receiver (Rx) pad that is attached underneath an EV [21]. One of the main challenges associated with DWPT networks lies in investigating the various operating point parameters to increase the systems' efficiency to transfer electrical power [22], [23]. This process can be computationally burdensome as the DWPT becomes more complex (i.e., as the system increases in scale). Zakerian et al. [24] developed a frequency tracking and voltage regulation model for a DWPT network to increase the efficiency and power factor in connection with the grid and achieved a higher efficiency approximately 72% of the time when compared to conventional methods and their study considered only one Tx pad within the modulation. Likewise, Xue et al. [25] validated a design for a 120 kW DWPT system of one Tx pad achieving 91.31% efficiency to deliver energy to the EVs battery system. Varghese et al. [26] assumed an EV velocity of 1600 km/h to reduce the computational burden during the proposed simulation of a three Rx pad architecture, which aimed to simplify the adoption of varying duty classes of EVs in DWPT networks. Inoue et al. [27] developed an optimization algorithm that utilized artificial neural networks to predict the output power of a DWPT network with four Tx pads and was capable of achieving an accuracy of 87.3% while also reducing data collection time from 40 months to 1 month, however, the scalability of their method is computationally burdensome when the number of Tx pads increases since the dataset necessary to train the model will increase proportionally with the length of the DWPT network. Reference [28] presented a DWPT model for three separate Tx pad configurations all consisting of multiple lengths and dimensions for a roadway length of 1 km by considering groupings of EVs throughout the charging system. Debnath et al. [29] explored the electromagnetic transient behavior of a 30 mile DWPT network by considering a constant velocity and one duty class of EVs.

In the context of DWPT networks, the majority of research is found to be primarily focused on small-scaled systems when the need to have high accuracy is required to analyze switching transients, although that produces high computational burden because the time-scale of simulations can range from nanoseconds to milliseconds. When considering a constant EV Traffic Flow (TF) through a DWPT or

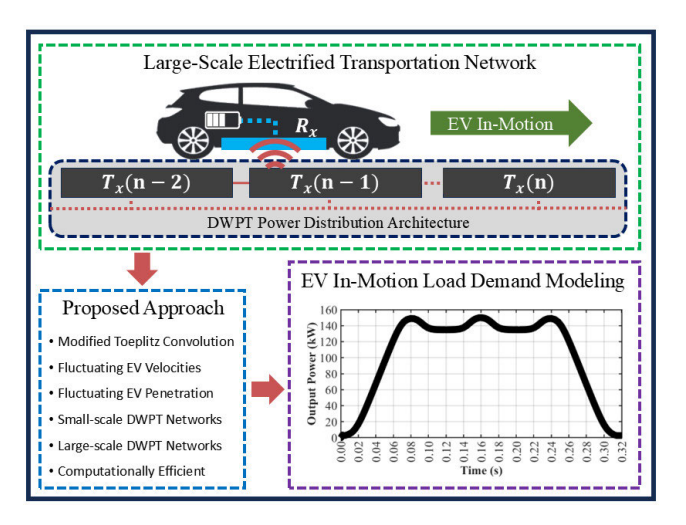


FIGURE 1. Overview of proposed approach for DWPT network load demand modeling.

a constant velocity for the EVs, the processing intensity reduces and that also deteriorates the performance of the model to generate more accurate load demand profiles since real-world applications will have fluctuating TF and velocities. In these applications, switching transients are lost due to the assumption of constant energy transfer. Furthermore, as the length of the DWPT roadway increases, the complexity of the data required to simulate higher integration of Tx pads accurately intensifies proportionally, thus amplifying the processing time when switching transients are of concern.

The limited scalability of DWPT network research in literature presents a need to further explore convincing methodologies to achieve more reduced computational intensity while achieving higher accuracy in order to perform impact analyses from large-scale DWPT roadway on the electric power distribution grid. In our previous work [30], an Integrative (INTG) object-oriented algorithm was developed to analyze different DWPT network lengths in conjunction with the fluctuation of EV TF and velocities, assuming a constant energy transfer while the EVs are traversing over the DWPT roadway. This paper presents a novel Convolution (CONV) method with scalability and light computational load to achieve more accurate modeling of power and energy profiles for (i) any given DWPT roadway with varying EV TF, (ii) dynamically fluctuating velocities, and (iii) the dimensional characteristics of the charging infrastructure. References [31], [32], and [33] demonstrated the theory of discrete linear CONV utilizing the Toeplitz method, however, in this paper, our proposed CONV modifies the matrices to mimic the traversal of EVs through a DWPT network to generate power output profiles from the overlapping of the Tx and Rx pads through time; thus, hereinafter, our proposed modified Toeplitz CONV method will be termed as mCONV. To the best knowledge of the authors, a mCONV method to calculate DWPT network load demands does not exist in the current literature, thus making this paper novel. Fig. 1 presents the scope of this paper to model small-scale and large-scale DWPT network load demands utilizing the proposed *mCONV*, fluctuating EV velocities, and varying EV densities. Hence, in contrast to the existing literature, the major contributions of this paper lies in the following: (1) Development of a new and an effective methodology for accurately modeling the power and energy profiles of large-scale DWPT networks with significantly reduced computational intensity and detailed dimensional characteristics of DWPT roadways, (2) Comprehensive analyses comparing different methods in generating DWPT load demand profiles, and (3) Advancing the field of electrified transportation, particularly in regards to EV in-motion charging systems of the future.

The remainder of this paper is organized as follows. Section II presents the proposed *mCONV* method to model the load demand of a large-scale DWPT roadway system. Section III provides a validation of our proposed method on a small-scale DWPT system by comparing its results with those obtained from power electronics simulation. Section IV demonstrates the load modeling of large-scale DWPT roadway with real-world TF data using the proposed method. Section V concludes the major findings of the paper.

II. PROPOSED mCONV METHOD

This section describes the development of the proposed novel method to generate DWPT load demands utilizing a *mCONV* method that accounts for the dimensions of the charging system and varying density and velocities of EVs.

A. FRAMEWORK OF CONVOLUTION METHOD

In DWPT networks, the motion of the Rx pad with respect to the Tx pad through time can be conceptualized as two overlapping objects that produce various power outputs according to the cross-sectional area between them. Likewise, the theory of convolution is a mathematical formulation that combines two distinct functions by overlapping them and finding the cross-sectional area to produce a representative result of both functions. The relationship between the Rx and Tx pads can be expressed by linearly time invariant functions when the EVs velocity at this junction is not considered, which results into a discrete convolution expression defined as:

$$P_{y}[n] = S_{R}[n] * S_{T}[n] = \sum_{i=0}^{N} S_{T}[i] S_{R}[n-i], \qquad (1)$$

where S_R is the characteristics of the Rx pads on EVs, S_T is the characteristics of the DWPT network, n is the length of the charging system, N is the current position of overlap, and y is the output matrix that contains the cross-sectional areas according to position in the roadway. The relationship between the Rx and Tx pads can be further constructed as a diagonally constant matrix that allows for a simplification by



utilizing a Toeplitz matrix.

$$T_{R} = \begin{bmatrix} 0 & 0 & 0 & \dots & 0 \\ S_{R}[0] & 0 & 0 & \dots & 0 \\ S_{R}[1] & S_{R}[0] & 0 & \dots & 0 \\ S_{R}[2] & S_{R}[1] & S_{R}[0] & \dots & 0 \\ 0 & S_{R}[2] & S_{R}[1] & \dots & 0 \\ 0 & 0 & S_{R}[2] & \dots & 0 \\ \vdots & \vdots & \vdots & \ddots & \vdots \\ \vdots & \vdots & \vdots & \ddots & \vdots \\ \vdots & \vdots & \vdots & \dots & S_{R}[\delta] \\ 0 & 0 & 0 & 0 & 0 \end{bmatrix}$$

$$S_{T} = \begin{bmatrix} S_{T}(1) \\ S_{T}(2) \\ S_{T}(3) \\ \vdots \\ S_{T}(n) \end{bmatrix}$$

$$P_{V} = [T_{R}, S_{T}], \rho \qquad (4)$$

In (2), the motion of the Rx pad is constructed utilizing a mCONV matrix designed to track the movement of the EV as it traverses across the DWPT network, where δ is the dimensional length of the Rx pad, the rows represent the different positions of the Rx pad, and the columns are the length of the DWPT network. Therefore, T_R is constructed as a m-by-n matrix instead of the defined n-by-n dimensions of Toeplitz, where n is the length of the DWPT network and m is the distance for the EV to traverse through the entire charging system. In (3), the matrix S_T is comprised of the dimensional characteristics of the DWPT network where the physical lengths, number of Tx pads, and the gaps between each Tx pad are considered. By utilizing (2) and (3), the resulting P_{ν} matrix can be calculated following (4) where the additional variable ρ is implemented to convert the output matrix from position/ cross-sectional area to position/ power output. Since P_{ν} is a function of position and power output, the EVs velocity can then be used to determine how much energy is being transferred over time.

B. DEVELOPMENT OF CONVOLUTION BASED METHOD

In this subsection, the mCONV method is further elucidated through visual representation to demonstrate how the matrices are developed/utilized to generate load demand profiles for a DWPT network. Fig. 2(a) illustrates how the S_R and S_T arrays are implemented with each having a particular length depending on their own specifications. For the S_R matrix, in this case, the length (δ) comprises of three colors (i.e., orange, blue, and green) with each representing a unit of length. For the S_T matrix, the length of each individual Tx pad (α) and the gap distance (λ) between them are considered (i.e., dark blue and white colors respectively) with each color representing a unit of length. The unit of length between S_T and S_R must be consistent as the indices need to align properly for the mCONV method to function. In Fig. 2(b), the S_R matrix is utilized to develop the mCONV. The left-hand side of Fig. 2(b) illustrates how the S_R matrix is positioned through

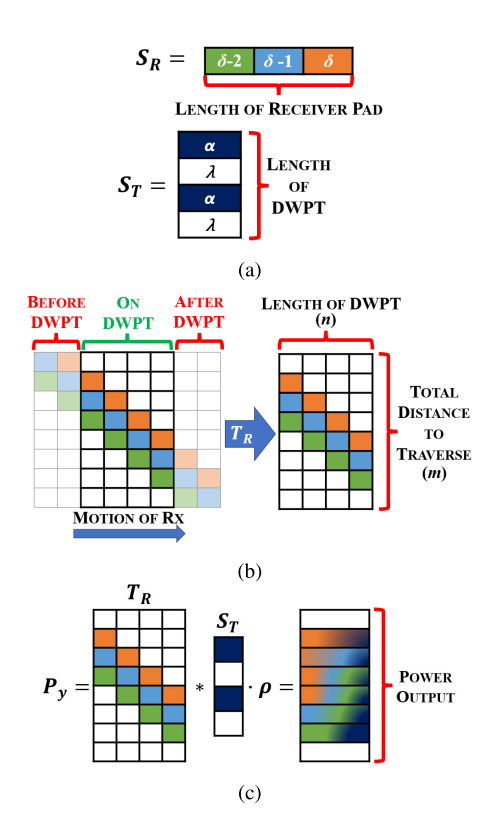


FIGURE 2. Modified Toeplitz convolution (mCONV) method for DWPT load demand approximation: (a) Rx and Tx pattern, (b) mCONV, and (c) cross-sectional area power output array.

each row to simulate the traversal of an EV through the DWPT network. Then, on the right-hand side of Fig. 2(b), the resulting mCONV matrix is presented. The columns represent specific units of length, which must equal in numbering to the overall length of the DWPT network. The rows represent the S_R traversal through the system, thus the first and last rows account for positions before and after the DWPT network. Fig. 2(c) visualizes how the linear multiplication of T_R , S_T , and ρ is implemented to generate power outputs. Each index in P_y represents a unit of length and each value—in this case gradient colors—provides the power output expected at each position. The matrix P_y can thereby be utilized in a simulation of an EV traversing a DWPT network where velocity and its position through time can be considered to determine the energy transference.

C. CONVOLUTION ALGORITHM FOR DWPT LOAD MODELING

As demonstrated in the previous subsection, the process to generate DWPT load demands utilizing the mCONV method requires three separate stages. The first stage, presented in Algorithm 1, is to generate the DWPT characteristic profile as the length of the charging system must be known to generate the mCONV matrix. Rows 1 through 7 of Algorithm 1 produces a temporary array that contains a single $Tx(\alpha)$ with magnitude equal to the capacity limits (β') of the Tx pad and the gap distance (λ) between consecutive pads. Rows



Algorithm 1 Produce DWPT Transmitter Pad Profile

Input: Dimensions of DWPT transportation network. **Output:** Transmitter pad profile.

```
1: for i=1:1:(\alpha+\lambda) do
 2:
        if i < 1 then
 3:
            temp(i,1) = \beta'
        else
 4:
            temp(i,1) = 0
 5:
        end if
 6:
 7: end for
 8: N = (n + 1)/\text{size(temp)}
 9: \epsilon = \operatorname{ones}(N,1)
10: for j=1:1:N do
11:
        s = size(S_T)
        if s(1) > x then
12:
13:
            break
        else
14:
            S_T = \operatorname{vertcat}(S_T, \operatorname{temp}^* \epsilon(j))
15:
16:
        end if
17: end for
18: return S_T
```

8 through 17 concatenate the temporary array upon itself a number of times N in order to produce a S_T matrix that is of equal length of the DWPT network. Row 9 of Algorithm 1 produces an array (ϵ) equal in size to the number of Tx pads within the DWPT network, where each value represents a percentage of horizontal overlap to account for the widths of the Rx and Tx pads. The second stage develops the mCONV matrix by utilizing the S_T from Algorithm 1. Rows 1 through 4 of Algorithm 2 generate the profile for the S_R matrix according to the dimension specifications of the Rx pad (δ) and its charging capacity limit (β) . Row 5 of Algorithm 2 then utilizes the length (n) of the S_T to produce an identity matrix. Rows 6 through 14 develop the mCONV matrix by inserting the S_R pattern at every instance where the value is equal to one. This process generates the m-by-n matrix for the mCONV method where m is the distance the EV needs to traverse and n is length of the DWPT network.

Fig. 3 illustrates the appearance of the S_T and S_R matrices after Algorithms 1 and 2 are performed, where δ is the length of the Rx pad, α is the length of the Tx pad, λ is the gap distances between consecutive Tx pads, β is the charging capacity limit of the Rx pad, β' is the capacity limit of the Tx pads, and ϵ is the operating point percentage that accounts for the displacement between the Rx and Tx pads during lane drifting of EVs. The differences in magnitude between the S_T and S_R matrices demonstrate the flexibility of the method to restrict the amount of energy transferred according to the capacity limits of the Tx pads. Thus, for instance, if the Rx pad had a power capacity limit beyond the Tx pad, then the maximum amount of power that the Rx pad would receive is limited according to the Tx pad capacity. Conversely, if the Tx pad has a higher capacity limit than the Rx pad, then the

Algorithm 2 Produce *mCONV* Matrix

```
Input: Transmitter pad profile S_T.
Output: mCONV matrix.
 1: S_R = zeros(\delta, 1)
 2: for i=2:1:(\delta+1) do
       S_R = \beta
 3:
 4: end for
 5: T_R = \exp(n, n)
 6: for j=1:1:n do
 7:
       x = 0
 8:
       for k=1:1:\delta do
          T_R(j+x,j) = S_R(k,1)
 9:
10:
11:
       end for
12: end for
13: A = zeros(1, n)
14: T_R(end + 1, :) = A;
15: return T_R
```

Algorithm 3 Produce DWPT Output Power Profile

Input: Transmitter pattern S_T and Toeplitz matrix T_R . **Output:** Output load demand P_R matrix.

```
1: P_A = T_R * S_T

2: [\max, \sim] = \max(P_A)

3: \rho = 0

4: if \beta \ge \beta' then

5: \rho = \beta'/\max

6: else

7: \rho = \beta/\max

8: end if

9: return (T_R * S_T)\rho
```

Rx pad would be restricted to its own maximum capacity. Additionally, in Fig. 3, the x-axis is in units of length, such as centimeter or millimeter, and the y-axis is in units of Watts according to the rated power of the Rx and Tx pads. The yellow highlighted regions in Fig. 3 demonstrates the convolution of the S_T and S_R matrices to produce the P_y output matrix. In row 1 of Algorithm 3, the mCONV method is implemented to generate the cross-sectional areas between the S_T and S_R matrices. Rows 2 through 8 determine the maximum cross-sectional area produced and then calculates the fitting variable to convert the output results from position/ cross-sectional area to position/ power output. At row 9 of Algorithm 3, the final P_v output matrix is produced for a single EV's traversal across the DWPT network. Fig. 4 presents the P_{ν} matrix results where the x-axis is the position across the DWPT network and the y-axis is the power output.

In Fig. 5, a comprehensive flowchart of the mCONV method is illustrated to demonstrate how DWPT network load demands are calculated. Steps 1 and 2 are utilized to determine the specifications of the charging network and the EV. Step 3 produces the matrices S_T and S_R that is then implemented in Step 4 to develop the T_R matrix. Step 5 will



produce the output matrix P_y that represents the output power per unit of distance. Step 6 determines the velocity of the EV that is traversing the DWPT network, which is then utilized in Step 7 to calculate the output power according to the position of the EV through time from the P_y matrix.

III. VALIDATION OF mCONV METHOD THROUGH POWER ELECTRONIC SIMULATION

This section presents the validation procedure for the proposed *mCONV* method through power electronic-based simulation of a small-scale (three Tx pads) DWPT network. Two other methodologies are presented to provide thorough comparison of the available approaches in literature to determine the computational intensity (i.e., reduced processing time) while also maintaining accuracy.

A. DESCRIPTION OF POWER TRANSMITTERS

A DWPT network can be established in several different power distribution architectures to facilitate the power transfer from the grid to EVs as they are traversing. These include, but not limited to, ac voltage distribution, dc voltage distribution, and dc current distribution [34]. This paper considers a dc voltage distribution for the DWPT network where a single grid-connected ac/dc converter provides the dc voltage to the Power Transmitter (PT) that generates the high-frequency current running through the Tx pad. Multiple PTs are connected in parallel to the output of the ac/dc converter as shown in Fig. 6. Each PT in the DWPT system is an active full bridge that generates an 85 kHz high-frequency square wave as illustrated in Fig. 7. In current literature, several passive compensation networks are available to be implemented in DWPT networks [23], [35], [36], [37]. In this paper, a dual-LCCL tuning topology is used in the system for its load-independent transmitter current characteristics. A diode rectifier is used on the receiver side before connecting to the battery. Through inductive coupling, energy is exchanged between the Tx pads and Rx pads as current flows through the Tx pad. The amount of power transferred is proportional to the coupling factor between the pads. Furthermore, the power transfer can be controlled by changing the phase shift ϕ between the two half-bridge legs. In Fig. 7, L_s is the Rx pad and L_p represents one of the Tx pads of the DWPT system. The LCCL compensation used in this paper is designed by following the validated methodology available in [38]. Additionally, this paper utilizes the split-tuning design as presented in [39].

In the DWPT system, the coupling factor between the Tx and Rx pads changes as the vehicle travels down the roadway. The coupling factor is represented as

$$k_{ij} = \frac{M_{ij}}{\sqrt{L_i L_j}},\tag{5}$$

where i and j are the identifiers of the two pads in question, M_{ij} is the mutual inductance between the two pads, and L_i and L_j are the self-inductances of the individual pads, respectively. For the system under consideration (see Fig. 6) with three Tx

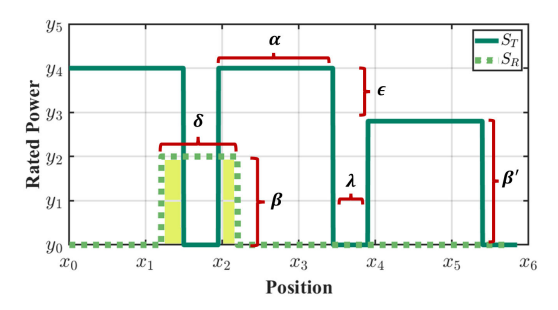


FIGURE 3. Transmitter and receiver pad profiles (δ is the length of the Rx, α is the length of the Tx, λ is the gap between each Tx, β is the charging capacity limit of the Rx pad, β' is the capacity limit of the Tx pads, and ϵ is the operating point percentage of pad overlap).

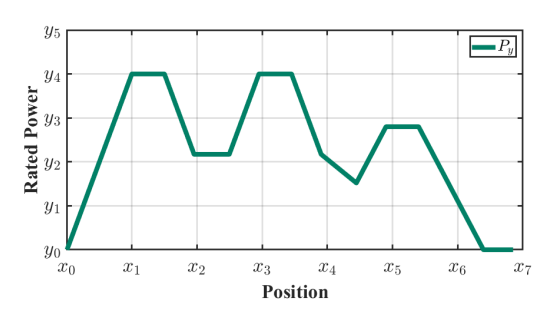


FIGURE 4. Power demands from convolution method according to EV position on the DWPT network.

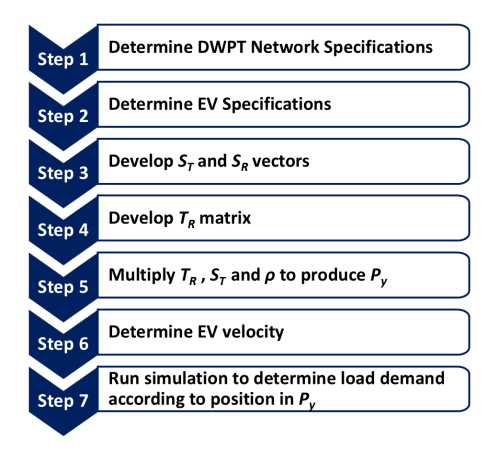


FIGURE 5. Diagram of mCONV algorithmic flow.

pads (represented by Pad 1, Pad 2, and Pad 3) and one Rx pad (represented by Pad 4), the inductance matrix is given by

$$\mathbf{L} = \begin{bmatrix} L_1 & M_{12} & M_{13} & M_{14} \\ M_{12} & L_2 & M_{23} & M_{24} \\ M_{13} & M_{23} & L_3 & M_{34} \\ M_{14} & M_{24} & M_{34} & L_4 \end{bmatrix}.$$
(6)

B. POWER ELECTRONIC-BASED DWPT SIMULATION

To obtain the desired simulation results for the DWPT network, this work follows the validated simulation process exhibited in [38] and [39] where three separate simulation stages are performed. *First*, a position-varying inductance matrix needs to be generated using Ansys Maxwell software,



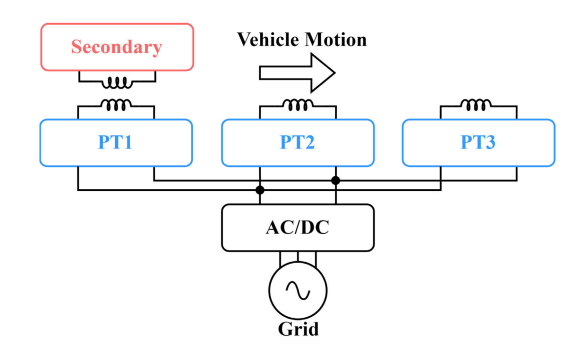


FIGURE 6. System diagram of small-scale DWPT simulations.

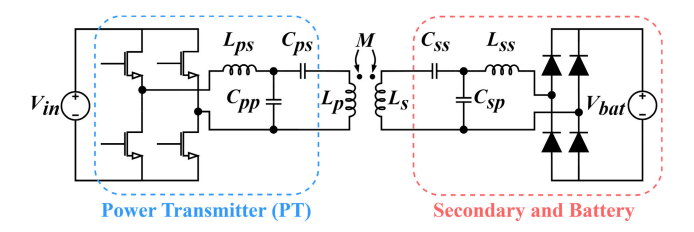


FIGURE 7. Circuit topology used in small-scale simulations of DWPT using power electronics.

which is commonly used to simulate magnetic designs for wireless power transfer. *Second*, the position-varying inductance matrix is converted into a time-varying matrix using MATLAB to be used as an input for the variable-inductor component in the *third* step that focuses on simulating a DWPT network in PLECS. Fig. 8 illustrates the processes (through Ansys, MATLAB, and PLECS) required to simulate DWPT networks, in particular PLECS assists to generate the load demand profiles that can be compared to the results obtained through the proposed *mCONV* method.

1) ANSYS INDUCTANCE MATRIX DESCRIPTION

The purpose of the Ansys simulation is to obtain a position-varying inductance matrix of the DWPT network for different Rx pad positions relative to the Tx pads. This matrix represents the coupling between all pads in the system as the Rx pad traverses over the Tx pads. The power transferred through the DWPT network is a function of the coupling between the Rx and Tx pads, e.g., when the Rx pad is directly aligned with the first Tx pad, the coupling factor and the power transferred are maximized. When the Rx pad moves away from the first Tx pad, the coupling factor and the power transferred will reduce. In Ansys, the Double-D (DD) shaped Tx and Rx pads are first created and placed at appropriate positions in the simulation space. Fig. 9 illustrates the simulation space in Ansys, where three Tx pads and one Rx pad are included. Table 1 presents a summary of the parameters utilized in the Ansys simulation. The inductance profiles are obtained by performing a parametric sweep of the Rx pad position. At each position of the Rx pad, the self and mutual inductance profiles of the four pads are obtained to generate a L matrix corresponding to the position

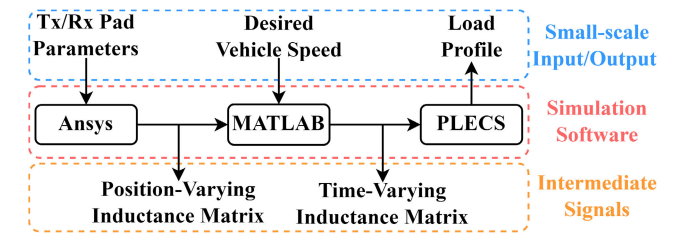


FIGURE 8. Workflow of DWPT simulations in power electronics.

of the Rx pad. Collectively, these L matrices generate the position-varying inductance matrix as shown in [38].

2) MATLAB AND PLECS SIMULATION DESCRIPTION

The position-varying inductance matrix generated from the Ansys simulation is then converted to a time-varying matrix using the designated vehicle velocity, which is given by

$$t_i = \frac{x_i - x_{min}}{V},\tag{7}$$

where x_i and x_{min} represent the current position of the Rx pad and the starting position of the Rx pad available from Ansys, respectively; V is the designated vehicle velocity; and t_i is the time when the Rx pad is at position x_i . Once each entry in the position-varying matrix is converted to a time-varying domain, the data is formatted for the variable-inductor component in PLECS as outlined in [38]. Fig. 10 shows the time-varying coupling coefficients in the considered system for any given vehicle velocity. Table 1 lists the parameters pertaining to the PLECS simulation for which an ideal voltage source (instead of a grid-connected ac/dc converter) is used as input for each PT. Using the properly-formatted time-varying inductance matrix obtained from the Ansys simulation (from Fig. 6), accurately accounts for the coupling between the Rx pad and each Tx pad at each simulation time step in PLECS. The PLECS simulation results thus produce the power transferred to the vehicle side of the DWPT network, and accordingly the load profiles are obtained.

C. VALIDATION DESCRIPTION OF PROPOSED CONVOLUTION METHOD

To accurately compare the proposed *mCONV* and INTG (our previous work [30]) methods, each time-step generated from the Ansys and PLECS simulation is utilized to model the power output profile of an EV. The same parameters, as presented in Table 1, are implemented to ensure an adequate comparison to perform the Ansys and PLECS simulations. Furthermore, the INTG method assumes that the maximum power is transferred to the EV as it traverses through the DWPT network. In this paper, the Ansys and PLECS simulations are implemented as a baseline to compare the accuracy and efficiency of the proposed *mCONV* method as they are recognized in literature for their better match to physical systems. Therefore, the *mCONV* and INTG methods are validated through the use of Mean Absolute



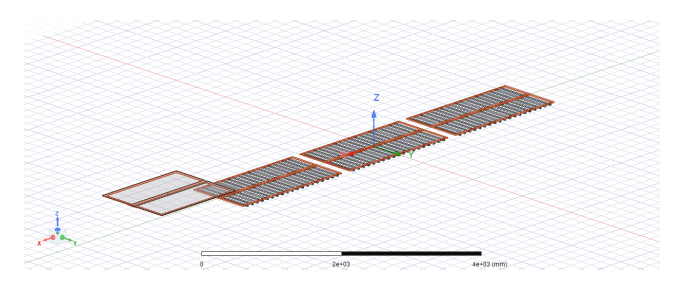


FIGURE 9. Ansys simulation model used to generate the time-varying inductance matrix used in PLECS.

Error (MAE) and Euclidean Similarity (ES) to measure the accuracy of the proposed *mCONV* and INTG methods through comparison with Ansys and PLECS simulation results while the efficiency is determined based upon the computational intensity to obtain the DWPT network load demand. The MAE and ES are calculated by

$$MAE = \frac{1}{n} \sum_{n=1}^{n} |Y_i - \hat{X}_i|,$$
 (8)

$$ES = \sqrt{\sum_{n=1}^{n} (Y_i - \hat{X}_i)^2},$$
 (9)

where Y represents the results of the Ansys and PLECS simulations, and \hat{X} represents either the INTG or the proposed mCONV method results.

D. SMALL-SCALE DWPT RESULTS: COMPARISON AND VALIDATION

To validate the performance of the INTG and mCONV methods, we compare their power output profiles obtained during the EV traversals across the DWPT network with those from the Ansys and PLECS simulations. Fig. 11 presents the results from each of the power profile methods (INTG, Ansys/PLECS, and mCONV) and demonstrates the effectiveness and accuracy of the proposed mCONV method. The INTG method (in red line) illustrates a clear deviation from the Ansys/PLECS simulation as it assumes a constant maximum power output while the EV is traversing across the DWPT network. The proposed mCONV method (in dotted green line) matches the baseline results from Ansys/PLECS simulations accurately and demonstrates a vast improvement in accuracy when compared to the INTG method as the fluctuations caused by the special gaps between each Tx pad are preserved. Table 2 presents the MAE and ES comparisons between mCONV (or INTG) with the Ansys and PLECS output power profile. As we can observe from both accuracy measures, test results demonstrated a significant reduction in error obtained from the mCONV method, thus outperforming the INTG method. The mCONV method has an MAE of approximately 2.2 kW, which is only 1.49% error on an average compared to the rated capacity of 150 kW. Moreover, the ES value (8.694 MWs) obtained from the mCONV method also showed its better performance than the INTG

TABLE 1. Parameters Utilized in Small-Scale DWPT Network.

Variables	Ansys	PLECS	mCONV
Tx Pad (α)	(2 x 1) m	_	2 m
$\operatorname{Rx}\operatorname{Pad}\left(\delta\right)$	(1.5 x 1.2) m	_	1.5 m
Horizontal Gap (λ)	0.1524 m	_	0.1524 m
Vertical Gap	0.305 m	_	_
EV Velocity	_	60 mph	60 mph
V_{in}	_	800 V	_
V_{bat}	_	800 V	_
Power (β', β)	_	150 kW	150 kW
L_{ps}	_	5.62 uH	_
C_{pp}	_	0.624 uF	_
$\stackrel{C_{pp}}{C_{ps}}$	_	0.424 uF	_
L_p	_	13.88 uH	_
L_s	_	11.85 uH	_
C_{ss}	_	0.413 u F	_
C_{sp}	_	1.05 uF	_
L_{ss}	_	3.35 uH	_
ϕ	_	165°	_
ϵ	_	_	100%

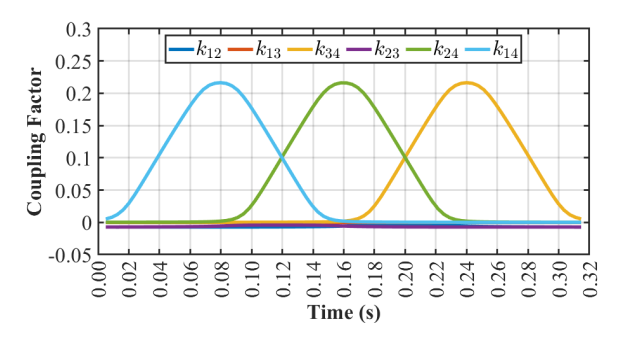


FIGURE 10. Coupling coefficients between all Tx and Rx pads in the small-scale DWPT simulation.

method with an improvement of approximately 93.67%. Table 3 presents the computational burden for each of the three methods where we can observe a massive reduction in the processing time for the *mCONV* (59.61 s) and INTG (0.203 s) methods when compared to the Ansys/PLECS simulation (26.880 ks). Although the INTG method has a reduced computational burden compared to the *mCONV* method, its accuracy, however, is much lower as seen in Table 2.

IV. LARGE-SCALE DWPT NETWORK LOAD MODELING

The previous section presented the results for a small-scale DWPT network comparing the INTG, *mCONV*, and Ansys/PLECS methods. In this section, a comparison between the INTG and *mCONV* methods for large-scale DWPT networks is performed to demonstrate the effectiveness of the proposed *mCONV* to reduce computational intensity while also maintaining a high level of accuracy. The results from Ansys/PLECS are not presented in this section due to their poor performance in terms of computational intensity that arises when simulating large-scale DWPT networks. For example, in a 1 mile DWPT network there are approximately 747 Tx pads when utilizing the dimensions in Table 1. Therefore, the processing time could potentially reach 77.53 days if an assumption is made that the



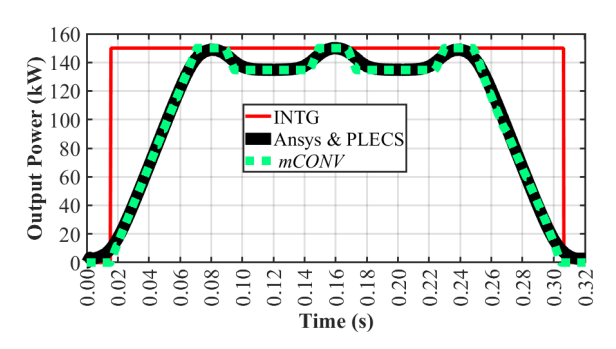


FIGURE 11. DWPT network power profile comparison results.

TABLE 2. Accuracy Metrics for DWPT Output Power Methods.

Method	MAE (W)	ES (MW)
mCONV	2,242.41	8.694
INTG	25,472.02	137.423

TABLE 3. Processing Intensity for Small-Scale DWPT.

Algorithmic Method	Processing Time (s)
mCONV	59.61
INTG	0.203
Ansys and PLECS	26,880

Ansys/PLECS software will perform linearly with the length of DWPT network compared to the results presented in Table 3. Accordingly, the validation metric of ES is modified which involves comparing only INTG and mCONV methods such that Y and \hat{X} in (9) now denotes the results from INTG and mCONV, respectively.

A. DATA DESCRIPTION FOR LARGE-SCALE DWPT MODELING

Since the accuracy of the proposed mCONV method has been validated in Section III, the purpose here is to compare our previously developed methodology [30], which implemented an object-oriented INTG method, with the proposed mCONV method. Fig. 12 presents the secondly TF that is utilized to determine the entry time of each EV into the DWPT network. This pattern was determined by calculating the averaged weekly seasonal vehicle counts for the i-10 gateway high in El Paso, TX during 2021 with an assumed EV density of 25% [40]. Table 4 presents a summary of the parameters utilized in the large-scale DWPT network simulations. Each EV will be randomly selected to either be a light-duty, medium-duty, or heavy-duty vehicle with each having varying charging capacities (i.e., the rating of the Rx pad) ranging from 50-80 kW, 100-170 kW, and 195-350 kW, respectively. Furthermore, the initial velocities of each EV is randomly selected from a range of 45-80 mph. These velocities are dynamically controlled at each secondly interval to ensure that the EVs cannot overlap each other on the single-lane charging system [30]. The DWPT network is simulated at five separate lengths from 2-10 miles in order to determine if the mCONV and INTG methods remain consistent with the calculated load demands and/or if the divergences between them increases/decreases proportionally.

B. LARGE-SCALE DWPT LOAD DEMAND MODELING RESUITS

Tables 5 through 7 present the comparison between the mCONV and the INTG methods for the large-scale DWPT networks for lengths ranging from 2 miles to 10 miles. The Ansys and PLECS methods are not considered in this scenario as the processing time would vastly exceed the small-scale DWPT result of approximately 7.5 hrs (i.e., 26,880 s) as presented in Table 3, which makes the Ansys/PLECS method unreasonable for large-scale simulations. However, the validity of the mCONV method to be utilized for large-scale DWPT networks is demonstrated through the formulation of the matrices implemented. Each matrix in the mCONV method is linearly increased based on the length of the DWPT network without changing any other parameter. Thus, the mCONV methods performance to achieve a more accurate load demand modeling compared to the INTG would result in similar behavior for small-scale or large-scale DWPT networks. Figs. 13(a) and (b) illustrate the modeled load demand profile for the 10 mile DWPT network utilizing the mCONV and INTG methods for a weekly and a daily period, respectively. In Figs. 13(a) and (b), the load demand generated by the INTG method is seen higher than that of the proposed mCONV method, primarily during peak TF times. Fig. 13(c) illustrates the secondly load demand differences between the mCONV and INTG to demonstrate that the divergence between them is significant as the maximum load demand difference is approximately 1.25 MW. Table 5 provides the total differences in the generated energy demands from the INTG and mCONV methods at each DWPT network length. As expected, the energy demands for both methods increase proportionally with the length of the charging system, however, each method has a significant difference in their generated energy demands. In Table 5, the energy demand differences for the weekly period has a minimum of 4.2 MWh and a maximum of 17.7 MWh for the 2 mile and 10 mile DWPT networks, respectively. The results in Table 5 also demonstrate that the divergence in the energy demand between mCONV and INTG methods increases directly proportional with the length of the DWPT network. At each DWPT length, the mCONV method produces a lower energy demand, which indicates the superior performance of the proposed mCONV method over the INTG method in terms of providing a more accurate energy demand which is also validated by the MAE values as seen in Table 2. Furthermore, Table 6 presents the differences (between mCONV and INTG) given by the ES for each scenario where the likeness between the mCONV and INTG methods reduces as the length of the DWPT network increases.



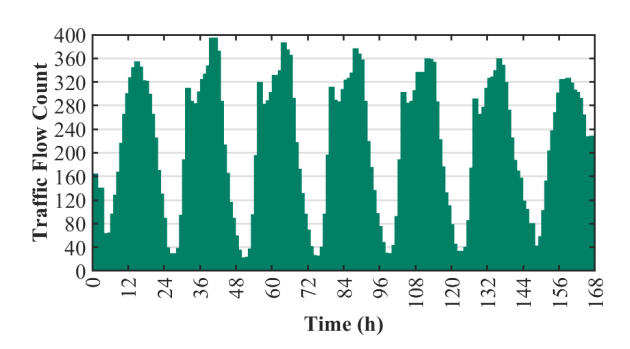


FIGURE 12. EV traffic flow counts for a weekly period.

TABLE 4. Parameters Utilized in Large-Scale DWPT Network.

Variables	mCONV & INTG
Rx pad limits (β)	50-350 kW
Tx pad limits (β')	350 kW
Length of Tx pad (α)	3 m
Length of Rx pad (μ)	1 m
Gap distance (λ)	0.025 m
Percentage of overlap (ϵ)	100%
Length of DWPT (n)	2-10 miles
EV velocities	40 - 80 mph
Intervals of simulation	1 second
Length of simulation	1 week

TABLE 5. Total Weekly Energy for Averaged Seasonal Traffic Flow.

DWPT Length	INTG (MWh)	mCONV (MWh)	Difference (MWh)
2 mile	111.9	107.7	4.2
4 mile	230.2	222.3	7.9
6 mile	349.0	337.0	12.0
8 mile	464.1	449.0	15.2
10 mile	573.9	556.2	17.7

TABLE 6. Euclidean Similarity Comparison for Large-Scale DWPT.

DWPT Length	ES (kW)
2 mile	9.2
4 mile	14.8
6 mile	22.3
8 mile	28.7
10 mile	34.7

Table 7 presents the minimum and maximum processing intensities (in seconds) for the weekly DWPT load demand where we can observe a minimal difference (i.e., 920.74 seconds and 895.30 seconds) between the *mCONV* and INTG methods. We can observe that these processing times are in sharp contrast to those (see Table 3) from the small-scale DWPT network when we consider the difference in the processing time between INTG and *mCONV* which can be elaborated as follows. For example, the small-scale results produced a processing time of 59.61 seconds (*mCONV*) and 0.203 seconds (INTG), and the difference between them is 59.407 seconds. Moreover, the processing times of 920.74 seconds (*mCONV*) and 895.30 seconds (INTG) are obtained for the large-scale simulations (see Table 7), thereby

TABLE 7. Processing Intensity for Large-Scale DWPT.

Algorithmic	Maximum	Minimum	Absolute
Method	Time (s)	Time (s)	Difference (s)
mCONV	4420.88	3500.14	920.74
INTG	4445.81	3550.51	895.30

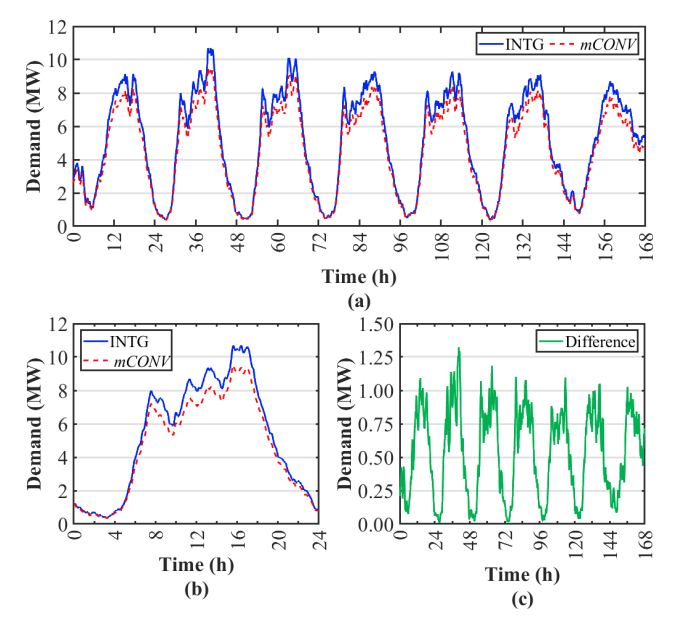


FIGURE 13. Comparison of *mCONV* and INTG 10 mile DWPT load demand profiles. (a) Weekly load demand, (b) Highest calculated daily load, and (c) Load demand difference between *mCONV* and INTG methods.

providing a difference of only 25.44 seconds. This clearly indicates that as the DWPT network length increases, the difference in the computational burden between the INTG and *mCONV* methods lessens.

C. COMPREHENSIVE DISCUSSION OF RESULTS

Test results demonstrated the accuracy and computational intensity of the proposed mCONV method that has a distinct advantage compared to the other methods. For small-scale DWPT roadway system, the mCONV method showed a higher degree in accuracy compared to the INTG especially by accounting for the spatial dimensions of the Tx pads, Rx pads, and the gaps between consecutive Tx pads. Furthermore, with respect to the computational intensity, we observed a massive improvement in processing time with the mCONV (59.61 seconds) showing superior performance than Ansys/PLECS (26,880 seconds), as shown in Table 8. This result is even more significant with respect to the use of processing architectures for the Ansys/PLECS and mCONV methods, i.e., in this paper, a computer architecture consisting of 128 GB of RAM and an AMD Ryzen Threadripper 2990WX 32-core processor was used for Ansys/PLECS, while the simulations for the proposed mCONV method are performed in an architecture of 16 GB of RAM and an Intel i7-8550U 4-core processor. Moreover, during the large-scale DWPT network modeling and analysis, the performance



TABLE 8. Comparative Overview of Processing Intensity Results for DWPT Network Simulations.

	Small-Scale	Large-Scale	Computer
Method	Processing	Processing Time	Processing
	Time (s)	(days)	Architecture
Ansys			AMD Ryzen
and	26,880	*110.3 - 551.7	Threadripper
PLECS			2990WX 32-core
INTG	0.203	0.04109 - 0.05146	Intel i7-8550U
mCONV	59.61	0.04051 - 0.05117	4-core

*Value is assumed based on small-scale results if processing of Ansys/PLECS has linear increase.

of both mCONV and INTG methods were found quite similar with respect to their computational intensity with the mCONV method displaying a higher accuracy than the INTG method, and the variance in load demand between them only increases proportionally with the length of the DWPT system. Additionally, if an assumption is made that the processing time for Ansys/PLECS increases linearly with the length of the DWPT network then the mCONV method is capable of reducing the computational burden from 110.3 days (i.e., with a single EV) to approximately an hour (i.e., with hundred of EVs) for a 2 mile network, as shown in Table 8. Therefore, if switching transients are of concern, then small-scaled DWPT networks should be performed utilizing the Ansys/PLECS, or similar software in like manner. However, if a large-scale DWPT network is of an interest and the switching transients are of no concern, then the proposed mCONV method is the best fit to provide more accurate and efficient results with low computational intensity.

V. CONCLUSION

This paper presented a novel mCONV method to calculate the load demand profiles generated by DWPT networks for both small and large scales. Our proposed mCONV method utilized the dimensional specifications of the Tx and Rx pads to calculate the cross-sectional areas of overlap through time as EVs traverse through the DWPT system. To determine an overall effectiveness of the proposed method, test results were validated through accuracy (using MAE and ES) and efficiency (computational intensity) measures by comparing mCONV with other methods: Ansys/PLECS and INTG. Small-scale and large-scale DWPT networks were simulated to demonstrate how the mCONV has a massive improvement in computational burden compared to the Ansys/PLECS and INTG methods to determine load demand profiles. Simulation results indicated that the proposed mCONV method is best suited for research in large-scale DWPT transportation networks to comprehend the complex behavior they may pose onto electric power grids. Test results also indicated that the Ansys/PLECS are more suitable methods than mCONV and INTG for a small-scale DWPT network analysis when transient effects are of interest.

To further enhance the proposed *mCONV* method, future work can be the implementation of Fourier series expansion

for square wave forms to generate the S_T and S_R matrices which could potentially produce smoother edges between the transitional cross-sectional areas to generate more accurate results to be utilized in electric power grid and transportation network behavior research.

REFERENCES

- [1] Int. Energy Agency. Global EV Outlook 2021. Accessed: Feb. 8, 2024. [Online]. Available: https://www.iea.org/reports/global-ev-outlook-2021
- [2] EV Volumes. Global EV Sales for 2023 H1. Accessed: Feb. 8, 2024.[Online]. Available: https://ev-volumes.com/news/ev/global-ev-sales-for-2023-h1/
- [3] M. Korpås, A. F. Flataker, H. Sæle, B. N. Torsæter, K. B. Lindberg, S. Jiang, Å. L. Sørensen, and A. Botterud, "Learning from the Norwegian electric vehicle success: An overview," *IEEE Power Energy Mag.*, vol. 21, no. 6, pp. 18–27, Nov. 2023.
- [4] J. Quiros-Tortos, L. Ochoa, and T. Butler, "How electric vehicles and the grid work together: Lessons learned from one of the largest electric vehicle trials in the world," *IEEE Power Energy Mag.*, vol. 16, no. 6, pp. 64–76, Nov. 2018.
- [5] Alternative Fuel Data Center. Costs Associated With Non-Residential Electric Vehicle Supply Equipment. Accessed: Feb. 8, 2024. [Online]. Available: https://afdc.energy.gov/files/u/publication/evse_cost_report_2015.pdf
- [6] U.S. Department of Transportation. Charger Types and Speeds. Accessed: Feb. 8, 2024. [Online]. Available: https://www.transportation.gov/rural/ev/toolkit/ev-basics/charging-speeds
- [7] T. Gnann, A.-L. Klingler, and M. Kühnbach, "The load shift potential of plug-in electric vehicles with different amounts of charging infrastructure," *J. Power Sources*, vol. 390, pp. 20–29, Jun. 2018.
- [8] M. Parchomiuk, A. Moradewicz, and H. Gawinski, "An overview of electric vehicles fast charging infrastructure," in *Proc. Prog. Appl. Electr. Eng. (PAEE)*, Jun. 2019, pp. 1–5.
- [9] F. Ahmad, M. S. Alam, and M. Asaad, "Developments in xEVs charging infrastructure and energy management system for smart microgrids including xEVs," *Sustain. Cities Soc.*, vol. 35, pp. 552–564, Nov. 2017.
- [10] D. Wang, J. Gao, P. Li, B. Wang, C. Zhang, and S. Saxena, "Modeling of plug-in electric vehicle travel patterns and charging load based on trip chain generation," *J. Power Sources*, vol. 359, pp. 468–479, Aug. 2017.
- [11] American Petroleum Institute. Service Station FAQs. Accessed: Feb. 8, 2024. [Online]. Available: https://www.api.org/oil-and-natural-gas/consumer-information/consumer-resources/service-station-faqs
- [12] U.S. Department of Energy. Alternative Fueling Station Locator. Accessed: Feb. 8, 2024. [Online]. Available: https://afdc.energy.gov/stations/#/find/nearest?country=U.S.&fuel=ELEC&evlevels=all
- [13] S. Lukic and Z. Pantic, "Cutting the cord: Static and dynamic inductive wireless charging of electric vehicles," *IEEE Electrific. Mag.*, vol. 1, no. 1, pp. 57–64, Sep. 2013.
- [14] U.S. Department of Energy. Alternative Fuels Data Center: Electric Vehicle Benefits and Considerations. Accessed: Feb. 8, 2024. [Online]. Available: https://afdc.energy.gov/fuels/electricity_benefits.html
- [15] F. Turki, V. Staudt, and A. Steimel, "Dynamic wireless EV charging fed from railway grid: Magnetic topology comparison," in *Proc. Int. Conf. Electr. Syst. Aircr., Railway, Ship Propuls. Road Vehicles (ESARS)*, Mar. 2015, pp. 1–8.
- [16] M. Waseem, M. Ahmad, A. Parveen, and M. Suhaib, "Battery technologies and functionality of battery management system for EVs: Current status, key challenges, and future prospectives," *J. Power Sources*, vol. 580, Oct. 2023, Art. no. 233349.
- [17] S. Maji, D. Etta, and K. K. Afridi, "A high-power large air-gap multi-MHz dynamic capacitive wireless power transfer system utilizing an active variable reactance rectifier for EV charging," in *Proc. IEEE Energy Convers. Congr. Expo. (ECCE)*, Oct. 2022, pp. 1–6.
- [18] R. M. Nimri, A. Kamineni, and R. Zane, "A modular pad design compatible with SAE J2954 for dynamic inductive power transfer," in *Proc. IEEE PELS Workshop Emerg. Technol., Wireless Power Transf.* (WoW), Nov. 2020, pp. 45–49.



- [19] A. Sagar, A. Kashyap, M. A. Nasab, S. Padmanaban, M. Bertoluzzo, A. Kumar, and F. Blaabjerg, "A comprehensive review of the recent development of wireless power transfer technologies for electric vehicle charging systems," *IEEE Access*, vol. 11, pp. 83703–83751, 2023.
- [20] J. Kracek and M. Svanda, "Analysis of capacitive wireless power transfer," IEEE Access, vol. 7, pp. 26678–26683, 2019.
- [21] A. Ahmad, M. S. Alam, and R. Chabaan, "A comprehensive review of wireless charging technologies for electric vehicles," *IEEE Trans. Transport. Electrific.*, vol. 4, no. 1, pp. 38–63, Mar. 2018.
- [22] K. V. V. S. R. Chowdary, K. Kumar, B. Nayak, A. Kumar, and M. Bertoluzzo, "Dynamic wireless charging performance enhancement for electric vehicles: Mutual inductance, power transfer capability, and efficiency," *Vehicles*, vol. 5, no. 4, pp. 1313–1327, Oct. 2023.
- [23] A. C. Bagchi, A. Kamineni, R. A. Zane, and R. Carlson, "Review and comparative analysis of topologies and control methods in dynamic wireless charging of electric vehicles," *IEEE J. Emerg. Sel. Topics Power Electron.*, vol. 9, no. 4, pp. 4947–4962, Aug. 2021.
- [24] A. Zakerian, S. Vaez-Zadeh, and A. Babaki, "A dynamic WPT system with high efficiency and high power factor for electric vehicles," *IEEE Trans. Power Electron.*, vol. 35, no. 7, pp. 6732–6740, Jul. 2020.
- [25] L. Xue, V. Galigekere, G.-J. Su, R. Zeng, M. Mohammad, E. Gurpinar, S. Chowdhury, and O. Onar, "Design and analysis of a 200 kW dynamic wireless charging system for electric vehicles," in *Proc. IEEE Appl. Power Electron. Conf. Exposit. (APEC)*, Mar. 2022, pp. 1096–1103.
- [26] B. J. Varghese, R. A. Zane, A. Kamineni, R. Tavakoli, Z. Pantic, C. Chou, and L. Liu, "Multi-pad receivers for high power dynamic wireless power transfer," in *Proc. IEEE Energy Convers. Congr. Expo. (ECCE)*, Oct. 2020, pp. 5162–5168.
- [27] S. Inoue, D. Goodrich, S. Saha, R. Nimri, A. Kamineni, N. S. Flann, and R. A. Zane, "Fast design optimization method utilizing a combination of artificial neural networks and genetic algorithms for dynamic inductive power transfer systems," *IEEE Open J. Power Electron.*, vol. 3, pp. 915–929, 2022.
- [28] A. D. Maharaj, S. Bahadoorsingh, C. Sharma, C. Powell, and G. E. Mahadeo, "A simulation study of dynamic wireless power transfer for EV charging versus regenerative braking in a Caribbean Island," in *Proc. IEEE/PES Transmiss. Distrib. Conf. Expo. (T&D)*, Apr. 2018, pp. 1–9.
- [29] S. Debnath, A. Foote, O. C. Onar, and M. Chinthavali, "Grid impact studies from dynamic wireless charging in smart automated highways," in *Proc. IEEE Transp. Electrific. Conf. Expo (ITEC)*, Jun. 2018, pp. 950–955.
- [30] T. Newbolt, P. Mandal, H. Wang, and R. Zane, "Sustainability of dynamic wireless power transfer roadway for in-motion electric vehicle charging," *IEEE Trans. Transport. Electrific.*, vol. 10, no. 1, pp. 1347–1362, May 2024.
- [31] C. L. Phillips, J. M. Parr, and E. A. Riskin, Signals, Systems, and Transforms, 4th ed., Upper Saddle River, NJ, USA: Pearson College Div, 2007.
- [32] J.-J. Huang and P. L. Dragotti, "Learning deep analysis dictionaries— Part II: Convolutional dictionaries," 2020, arXiv:2002.00022.
- [33] R. M. Gray. Toeplitz and Circulant Matrices: A Review. Accessed: Feb. 15, 2024. [Online]. Available: https://ee.stanford.edu/~gray/ toeplitz.pdf
- [34] M. Chawla, A. Zade, T. Newbolt, P. Mandal, A. Kamineni, H. Wang, and R. Zane, "Modeling and comparative analysis of power distribution architectures for large-scale electric vehicle in-motion wireless charging infrastructures," in *Proc. Wireless Power Week (WPW)*, Jul. 2022, pp. 887–892.
- [35] J. Zhao, T. Cai, S. Duan, H. Feng, C. Chen, and X. Zhang, "A general design method of primary compensation network for dynamic WPT system maintaining stable transmission power," *IEEE Trans. Power Electron.*, vol. 31, no. 12, pp. 8343–8358, Dec. 2016.
- [36] Q. Zhu, L. Wang, Y. Guo, C. Liao, and F. Li, "Applying LCC compensation network to dynamic wireless EV charging system," *IEEE Trans. Ind. Electron.*, vol. 63, no. 10, pp. 6557–6567, Oct. 2016.
- [37] G. de Freitas Lima and R. B. Godoy, "Modeling and prototype of a dynamic wireless charging system using LSPS compensation topology," *IEEE Trans. Ind. Appl.*, vol. 55, no. 1, pp. 786–793, Jan. 2019.
- [38] B. J. Varghese, "Roadway-embedded transmitters and multi-pad receivers for high power dynamic wireless power transfer," Ph.D. thesis, Dept. Elect. Comput. Eng., Utah State Univ., Logan, UT, USA, 2021.

- [39] J. B. Larsen, "Communication-less synchronous rectification for in motion wireless charging," M.S. thesis, Dept. Elect. Eng., Utah State Univ., Logan, UT, USA, 2023.
- [40] U.S. Department of Transportation. U.S. Traffic Volume Data. Accessed: Feb. 8, 2024. [Online]. Available: https://www.fhwa.dot.gov/policyinformation/tables/tmasdata/#v20



TRAVIS NEWBOLT (Graduate Student Member, IEEE) received the B.S. and M.S. degrees in electrical and computer engineering (ECE) from The University of Texas at El Paso (UTEP), El Paso, TX, USA, in 2021 and 2022, respectively. He is currently pursuing the Ph.D. degree with the Power and Renewable Energy Systems (PRES) Laboratory, ECE Department, UTEP, and the NSF Engineering Research Center for Advancing Sustainability through Powered Infrastructure for

Roadway Electrification (ASPIRE). He is a Graduate Research Assistant with the PRES Laboratory, ECE Department, UTEP; and the NSF Engineering Research Center for ASPIRE. His current research interests include EV charging infrastructures, power system dynamics and stability, distributed energy resources integration to the grids, and distribution grid operations.



MCKAY WAITE (Graduate Student Member, IEEE) received the B.S. degree in electrical engineering from Utah State University (USU), Logan, UT, USA, in 2023. He is currently pursuing the Ph.D. degree with the USU Power Electronics Laboratory and the NSF Engineering Research Center for Advancing Sustainability through Powered Infrastructure for Roadway Electrification (ASPIRE). He is a Graduate Research Assistant with the USU Power Electronics Laboratory and

the NSF Engineering Research Center for ASPIRE. He served as the Co-Team Lead for the Undergraduate Team from USU that won the Grand Prize at the IEEE International Future Energy Challenge (IFEC), in 2022. His current research interests include the design, modeling, and control of power converters for dynamic wireless EV charging.



PARAS MANDAL (Senior Member, IEEE) received the Ph.D. degree in electrical engineering from The University of the Ryukyus, Japan, in 2005. He is currently the Director of the Power and Renewable Energy Systems (PRES) Laboratory and a Professor of electrical and computer engineering with The University of Texas at El Paso, El Paso, TX, USA. He is the author of more than 200 technical publications. His current research interests include electrified

transportation, AI and ML applications to power systems and forecasting, electricity market operations, and data-driven algorithms for cyber-physical systems. He assumes different roles at IEEE PES.





HONGJIE WANG (Senior Member, IEEE) received the B.S. degree in electrical engineering from the University of Shanghai for Science and Technology, Shanghai, China, in 2009, the M.S. degree in electrical engineering from Shanghai Jiaotong University, Shanghai, in 2012, and the Ph.D. degree in electrical engineering from Utah State University (USU), Logan, UT, USA, in 2018. From 2012 to 2014, he was a Senior Researcher with China Electric Power Research Institute,

Beijing, China, working on intelligent high-voltage equipment development and standardization. After graduating in 2018, he was a Postdoctoral Researcher with USU, for one year, where he has been an Assistant Professor with the Department of Electrical and Computer Engineering, since 2019. At USU, he serves as the Co-Director of the USU's Power Electronics Laboratory. He has co-authored more than 50 peer-reviewed publications and six issued patents. His current research interests include dc power distribution, analysis, design, and control of resonant converters, extreme fast charging, grid interface power converters, health monitoring and diagnosis of power converters, second-life battery and battery management systems, and dynamic wireless power transfer for transportation electrification applications. He was a recipient of the National Science Foundation Career Award, in 2023. He was a recipient of the 2022 Researcher of the Year Award and the 2023 Outstanding Advisor of the Year Award from the Department of Electrical and Computer Engineering, USU; and the 2023 Undergraduate Research Mentor of the Year Award from the College of Engineering, USU.



REGAN ZANE (Senior Member, IEEE) received the Ph.D. degree in electrical engineering from the University of Colorado Boulder, Boulder, CO, USA

He is currently the David G. and Diann L. Sant Endowed Professor with the Department of Electrical and Computer Engineering, Utah State University; and the Director of the NSF Engineering Research Center for Advancing Sustainability through Powered Infrastructure for Roadway Elec-

trification (ASPIRE). Prior to joining USU, he was an Assistant Professor and an Associate Professor with Colorado Power Electronics Center, University of Colorado Boulder, and a Research Engineer with the GE Global Research Center, Niskayuna, NY, USA. He has co-authored more than 220 peer-reviewed publications and the textbook Digital Control of High-Frequency Switched-Mode Power Converters (New York, NY, USA: Wiley, 2015). He has more than 30 issued patents. His research interests include power electronics for electric vehicle charging infrastructure, including extreme fast charging and static and dynamic wireless charging, battery management systems, dc microgrids, grid-tied and grid-interactive converters, and grid integration of energy storage and renewable energy. He was a recipient of the 2004 National Science Foundation Career Award, the 2005 IEEE Microwave Best Paper Prize, the 2007 and 2009 IEEE Power Electronics Society Transactions Prize Letter Awards, the 2008 IEEE Power Electronics Society Richard M. Bass Outstanding Young Power Electronics Engineer Award, and the 2021 Utah State University Researcher of the Year Award. He was a recipient of the 2006 Inventor of the Year, the 2006 Provost Faculty Achievement, the 2008 John and Mercedes Peebles Innovation in Teaching, and the 2011 Holland Teaching Awards from the University of Colorado.

. . .